Numerical investigation of flow field and structure of a micro - axial turbine of ORC using R245fa

Hung-Chun Hsu[1], Yi-Chen Li[2], Jui-Ching Hsieh[3*]

[1] National Chin-Yi University of Technology, E-mail: peter607514@gmail.com

[2] Industrial Technology Research Institute, E-mail: liyichen@itri.org.tw

[3]National Chin-Yi University of Technology, E-mail: jchsieh@ncut.edu.tw

*Corresponding Author: jchsieh@ncut.edu.tw

ABSTRACT

Environmental damage has been gradually increasing over the past few decades owing to industrialization. In many countries, attempts have been made to reduce carbon emissions by employing energy-saving and sustainability methods, such as waste heat recovery and renewable energy, respectively. For low-grade waste heat recovery, the organic Rankine cycle is a typical thermo-electric conversion system. In the present study, a thermodynamic analysis showed that the output power, working fluid mass flow rate, inlet temperature, and inlet and outlet pressures of a turbo-expander were 12.57 kW, 1.6 kg/s, 70 ℃, 0.53 MPa, and 0.267 MPa, respectively. Moreover, the one- and three-dimensional geometries of the turbo-expander were analyzed by using aerodynamic and computational fluid dynamics software, respectively. Additionally, the effect of the tip clearance between the blade tip and casing on the performance, stress, and strain of the blade was investigated, and the tip clearance was varied from 0% to 10%, at an interval of 5%. The results showed that as the tip clearance increased, the shaft power, isentropic efficiency, stress, and strain decreased. In addition, the effect of the tip clearance on the isentropic efficiency and structure was higher in the range of 0-5% than that in the range of 5-10%. Finally, when the tip clearance was 5%, the shaft power and isentropic efficiency were 14.87 kW and 61.12%, respectively.

1 Introduction

Rapid industrialization has contributed to enormous energy consumption; fossil fuels have been widely used to meet the electricity requirements over the past few decades. However, burning fossil fuels produces carbon dioxide, which causes environmental deteriorations such as global warming. Thus, renewable energy and carbon reduction technology have been investigated by many researchers worldwide. Waste heat recovery technology such as the organic Rankine cycle (ORC) is being developed; it is an effective method for converting medium- and low-grade heat sources into usable power [1]. The basic ORC has four major components: pump, evaporator, expander, and condenser. The function of an expander is to transfer heat energy to the generator; hence, the performance of the ORC system is proportional to the output shaft power and the isentropic efficiency of the expander. The expander is primarily categorized into two types: volumetric type [2-4] and velocity type [5-7]. Varying the geometry of the turbine has been proven to influence its performance. Wu et al. [8] conducted various numerical investigations and determined that with an increase in the parabolic index (t), the efficiency of the rotor increased suddenly and then decreased gradually. The results proved that the efficiency of the rotor increased by 1% when t=1.95. Several researchers have evaluated the turbine performance by varying the design parameters. Song et al. [9] presented a one-dimensional analysis model for a radial inflow turbine in the ORC system. The radial inflow turbine efficiency was predicted based on the velocity triangle and loss models, rather than the constant efficiency assumption. The influence of the properties of the working fluid and the operating conditions of the system on the turbine performance was evaluated. The results were interpreted by comparing the model-predicted turbine efficiency and the constant turbine efficiency. The efficiency of the predicted turbine model was numerically proven to be higher than the constant turbine efficiency at an evaporation temperature of 71.85 ℃.

In realistic industrial applications, a tip clearance exists between the blade tip of the rotor and the

casing to allow rotor rotation and to ensure system reliability. The rotational shaft has an axial force due to the push of the high-pressure working fluid on the rotor. However, the shaft force is inversely affected by the gap. The effect of the tip clearance on the performance of the expander is similar to that of the shaft force. In the present study, the effect of the tip clearance on the performance of the turbine and the stress and strain of the blade was examined to determine the optimal value of the gap.

2 ORC system model

The ORC system is similar to the traditional Rankine cycle, which uses water as the working fluid. However, in this study, R245fa is used as the working fluid, and its physical and environmental properties are listed in Table 1 [10].

Table 1 Physical and environmental data of working fluid.

Items	R245fa
Critical temperature (℃)	154.06
Critical pressure (MPa)	3.65
GWP (yr)	950
ODP	0
ASHRAE safety group	B1

2.1 ORC system description

The configuration and processes of the ORC system are shown in Figure 1; a typical ORC system consists of a pump, an evaporator, an expander, and a condenser. The ORC can be divided into four processes. First, the working fluid leaves the condenser and is pressurized by the pump as a sub-cooled liquid (processes 1–2). Then, the working fluid flows into the evaporator to exchange heat with the heat source (processes 2–5). Subsequently, the working fluid flows into the expander for the expansion process and produces shaft power to drive the generator (processes 5–6). Finally, after the expansion, the low-pressure vapor is condensed by the cooling source in the condenser (processes 6–1).

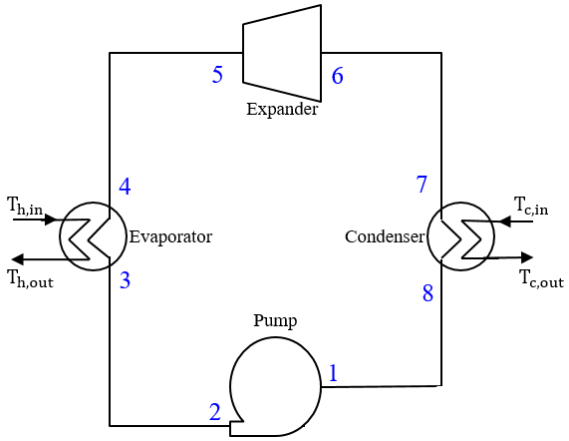

Figure 1 Configuration and processes of the ORC.

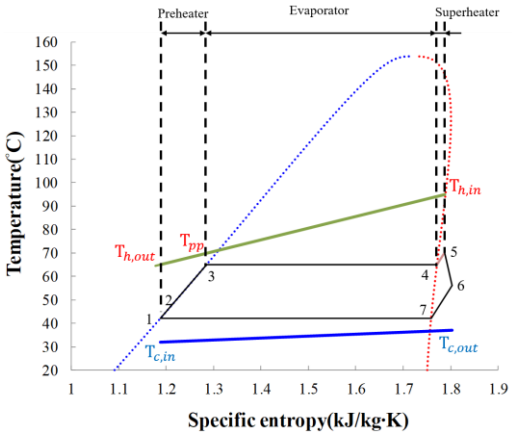

Figure 2 T-s diagram of the ORC.

2.2 ORC design conditions

The temperature-specific entropy diagram and design conditions are shown in Figure 2 and listed in Table 2, respectively. The heat source temperature, mass flow rate, and cooling source temperature are 95 ℃, 2.22 kg/s, and 32 ℃, respectively. Furthermore, the isentropic efficiencies of the pump, expander, and generator are 60%, 60%, and 90%, respectively.

Table 2 ORC design condition parameters.

Items	Parameters	Assumption
Heat source temperature (℃)	$T_{h,in}$	95

Cooling source temperature (℃)	$T_{c,in}$	32
Evaporation temperature(℃)	$T_{exp,in}$	65
Condensation temperature (℃)	$T_{cond,in}$	42
Temperature difference of pinch point in the eveporator (K)	$\Delta T_{pp,eva}$	5
Temperature difference of pinch point in the condenser (K)	$\Delta T_{pp,cond}$	5
Mass flow rate of heat source (kg/s)	$\dot{m}_h$	2.22
Pump isentropic efficiency (%)	η_p	60
Expander isentropic efficiency (%)	η_{exp}	60
Generator efficiency (%)	η_g	90

2.3 ORC thermodynamic model

The energy analysis model is designed based on the thermal efficiency of the thermodynamic cycle, and it was used to describe the conservation of energy. The energy analysis of each component can be expressed by using the following equations:

- Pump
  - Pump isentropic efficiency

$$\eta_{is}^{p} = \frac{h_{2,is} - h_1}{h_2 - h_1}, \tag{1}$$

where h is the enthalpy of the working fluid, subscripts 1 and 2 represent the inlet and outlet of the pump, respectively, and s is the isentropic entropy.

  - Pump power consumption

$$\dot{W}_p = \dot{m}_{wf}(h_2 - h_1) \tag{2}$$

- Evaporator
  - Heat load

$$\dot{Q}_h = \dot{m}_h\left(h_{h,in} - h_{h,out}\right) = \dot{m}_{wf}(h_5 - h_2) \tag{3}$$

Subscripts h, 5, and 2 represent the heat source, expander inlet, and pump outlet, respectively.

- Expander
  - Expander isentropic efficiency

$$\eta_{is}^{exp} = \frac{h_5 - h_6}{h_5 - h_{6s}} \tag{4}$$

Subscripts 5 and 6 denote the inlet and outlet of the expander, respectively, and s indicates the isentropic entropy.

  - Expander shaft power output

$$\dot{W}_{exp} = \dot{m}_{wf}(h_5 - h_6) \tag{5}$$

- Condenser
  - Cooling capacity

$$\dot{Q}_c = \dot{m}_c\left(h_{c,out} - h_{c,in}\right) = \dot{m}_{wf}(h_6 - h_1) \tag{6}$$

Subscripts c, 6, and 1 are the cooling source, expander outlet, and pump inlet, respectively.

- First law efficiency

$$\eta_I = \frac{\dot{W}_{net}}{\dot{Q}_h}, \tag{7}$$

where $\dot{W}_{net}$ is the expander-shaft power output after deducting the pump power consumption.

Based on the aforementioned design conditions, the performance of R245fa is evaluated by employing a thermodynamic model of the ORC system, which is developed by using MATLAB R2014B. The output data of the thermodynamic model are listed in Table 3.

Table 3 Output data of the thermodynamic model.

Items	Parameters	Value
Shaft power of expander (kW)	$\dot{W}_{exp}$	12.57
Consumed power of pump (kW)	$\dot{W}_{p}$	0.560
Net power output (kW)	$\dot{W}_{net}$	12.01
First law efficiency (%)	η_{I}	4.317
Mass flow rate of working fluid (kg/s)	$\dot{m}_{wf}$	1.639

The necessary data of the turbine in a one-dimensional aerodynamic model are obtained from the ORC design results of the thermodynamic model and are listed in Table 4.

Table 4 Boundary conditions of turbine

	Unit	Value
T_{in}	℃	70
P_{in}	MPa	0.53
P_{out}	MPa	0.267
$\dot{m}_{wf}$	kg/s	1.63
$\eta_{is,exp}$	%	60

3 Turbine analysis model

3.1 One-dimensional aerodynamic analysis

The first step in the design process is implemented by using a mathematical model in MATLAB, which guides the user to perform a preliminary sizing of the expander and evaluate its performance. The preliminary sizing and calculations of the turbine geometry are performed by using the ORC design conditions, such as pressure, temperature, mass flow rate, and isentropic efficiency (as shown in Table 4) and non-dimensional parameters, such as the degree of reaction, flow coefficient, and load coefficient. These parameters are combined with the one-dimensional aerodynamic equations to calculate the preliminary geometry of the blade. The aerodynamic equations are as follows:

- Mass conservation

$$\rho_1 A_1 V_1 = \rho_2 A_2 V_2 = \rho_3 A_3 V_3 \,, \tag{8}$$

where ρ is the density of the working fluid, A is the area of the cross section, V is the velocity of the working fluid, and subscripts 1, 2, and 3 are the inlet of the stator, interface of the stator and rotor, and outlet of the rotor, respectively.

- Energy conservation

$$\dot{Q} - \dot{W} = \dot{m}\left[(h_2 - h_1) + \frac{1}{2}(V_2^2 - V_1^2) + g(Z_2 - Z_1)\right], \tag{9}$$

where h is the enthalpy of the working fluid, g is the potential-energy unit mass flow rate, and $\dot{W}$ is the power.

- Euler turbomachinery equation

$$\dot{W} = \dot{m}U(V_{2t} - V_{1t}), \tag{10}$$

where U is the peripheral velocity at the mean blade radius, and subscript t is the tangential direction.

The blade of the stator and rotor is modeled by using the ANSYS BLADGEN® software. A computational grid is generated depending on the 3D blade profile and flow channels. A computational fluid dynamics (CFD) analysis of the turbine is conducted by using the ANSYS CFX® software. The effect of the tip clearance on the fluid flow and structure of the turbine is discussed, and a steady-state flow-field numerical simulation is used in this study.

3.2 Specific geometry parameters

The boundary conditions are combined with the aforementioned one-dimensional aerodynamic analysis to develop the specific geometry parameters and velocity triangle, which are presented in Table 5 and Figure 3, respectively.

Table 5 Specific geometry parameters.

Items	Unit	Value
r_{t1}	mm	95
r_{h1}	mm	91.5
r_{t2}	mm	95
r_{h2}	mm	89.7
r_{t3}	mm	95
r_{h3}	mm	87.7
α_1	degree	0
α_2	degree	73.49
β_2	degree	41.18
β_3	degree	-72.25

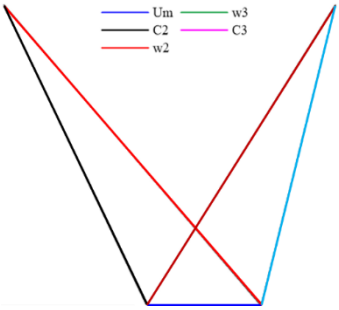

Figure 3 Velocity triangle

3.3 Numerical model

The boundary conditions of the turbo-expander can be obtained from the thermodynamic analysis, which includes the temperature and pressure of the inlet expander and the pressure of the outlet expander. The interfaces of the stator and rotor are connected by using a general grid interface. The CFD solver uses the finite volume method and second-order spatial accuracy level to solve the following three-dimensional steady-state Navier-Stokes equations:

- Continuity equation

$$\frac{\partial \rho}{\partial t} + \nabla \cdot (\rho U) = 0 \tag{11}$$

- Momentum equation

$$\frac{\partial (\rho \cdot U)}{\partial t} + \nabla \cdot (\rho U \cdot U) = -\nabla p + \nabla t \tag{12}$$

- Energy equation

$$\frac{\partial (\rho h_{tot})}{\partial t} - \frac{\partial p}{\partial t} + \nabla \cdot (\rho U h_{tot}) = \nabla \cdot (\lambda \nabla T) + \nabla \cdot (U \cdot \tau), \tag{13}$$

where τ and h_{tot} are stress tensor and total enthalpy, respectively.

Because the working fluid, R245fa, is not an ideal gas, the Aungier–Redlich–Kwong Real Gas model is used in this study:

$$P = \frac{RT}{v-b+c} - \frac{a(T)}{v(v+b)}\ , \tag{14}$$

where $a = a_0\left(\frac{T}{T_c}\right)^{0.4986+1.1735\omega+0.4757\omega^2}$, $b = \frac{0.08664\,RT_c}{p_c}$, $c = \frac{RT_c}{p_c+\frac{a_0}{v_c+(v_c+b)}} + b - v_c$, $a_0 = \frac{0.42747R^2T_c^2}{p_c}$, and ω is acentric factor.

The turbine blade geometry is shown in Figure 4. The computational grid is constructed by using a structured grid for spatial discretization. The total number of grids for the stator and rotor in the computational domain is approximately 66,120 and 78,330, respectively, as shown in Figure 5.

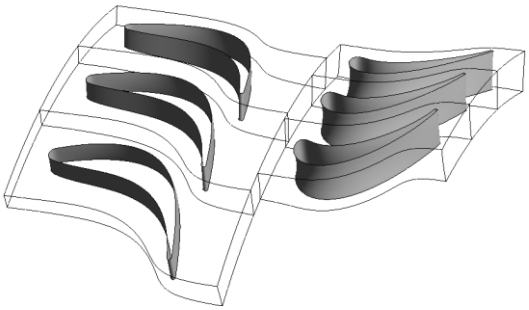

Figure 4 3D turbine blades.

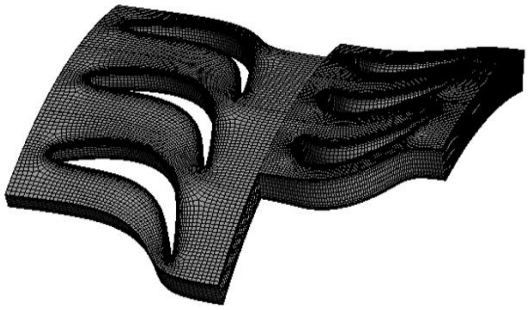

Figure 5 Computational grid for turbines.

4 Results and discussion

4.1 Effect of blade tip clearance on the performance

To evaluate the performance and structure of the turbine blade, CFD and structural analyses are conducted. Owing to the manufacturing tolerance and assembly of the blade, a gap exists between the blade tip and casing and is called the blade tip clearance. In this study, the effect of the rotor tip clearance on the performance and structure of the turbo-expander is examined. The clearance is varied from 0% to 10%, at an interval of 5%. Figure 6, Figure 7 and Figure 8 show the temperature, pressure, and Mach number stream field at the clearance of 0%, 5%, and 10%, respectively. The results show that the velocity of the stator is higher than that of the rotor owing to the relatively high pressure of the working fluid that flows into the narrow channel of the stator, thereby increasing the flow velocity. Therefore, the maximal velocity of the fluid flow appears at the outlet of the stator. Additionally, vortexes do not exist when the tip clearance is 0% and 5%. However, vortexes appear at the leading edge of the rotor, particularly as the tip clearance in the 10%.

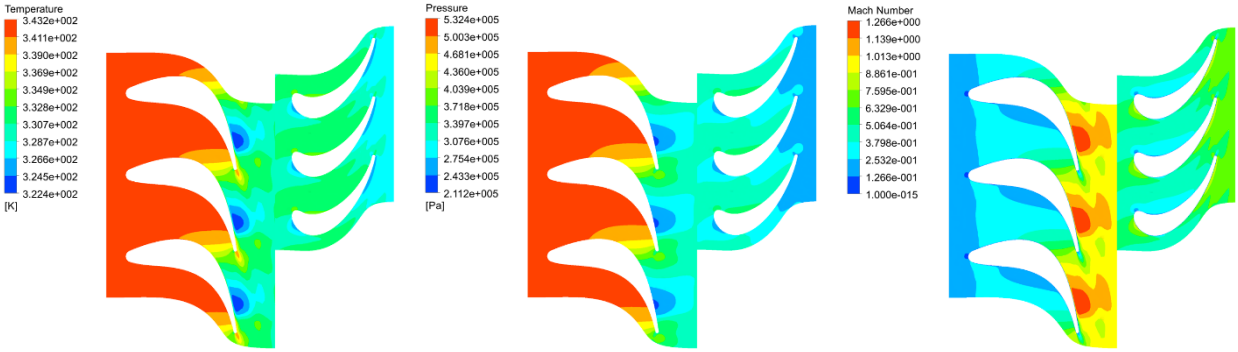

Figure 6 Temperature, pressure, and Mach number stream field of the clearance 0%.

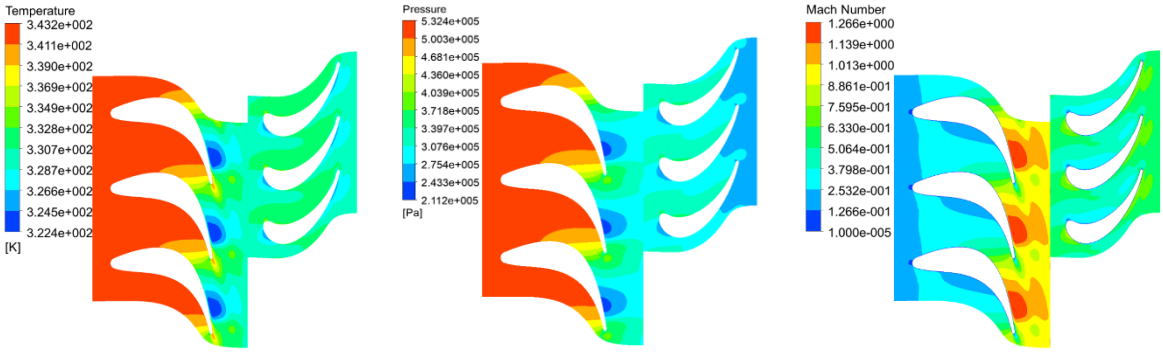

Figure 7 Temperature, pressure, and Mach number stream field of the clearance 5%.

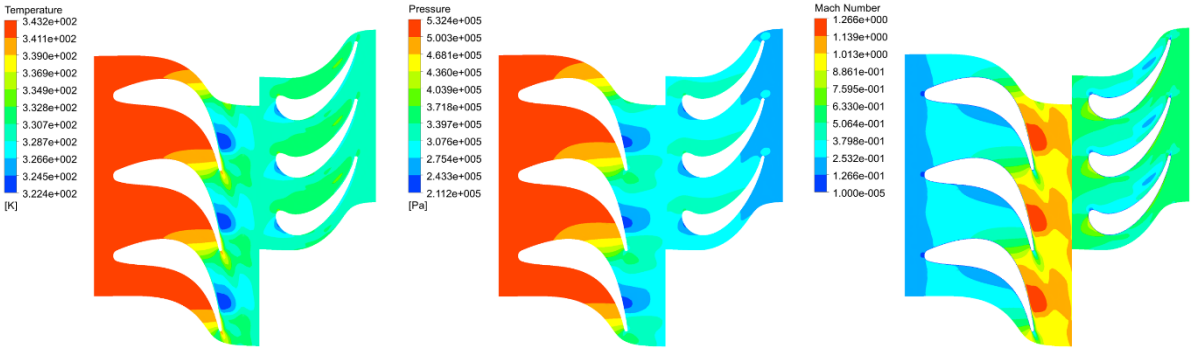

Figure 8 Temperature, pressure, and Mach number stream field of the clearance 10%.

Table 6 lists the output shaft power and the isentropic efficiency of the turbine. The results show that when a tip clearance exists, a fraction of the working fluid does not undergo expansion processes. Therefore, a part of the energy in the flow is lost, causing a decrease in the power and efficiency.

Table 5 Performance of the turbine at difference tip clearances.

Items	$\dot{m}_{wf}$(kg/s)	$\dot{W}_t$(kW)	η_{is}(%)
Design point	1.63	12.57	60
Tip clearance 0%	1.60	16.45	66.9
Tip clearance 5%	1.60	14.87	61.1
Tip clearance 10%	1.63	13.61	59.2

4.2 Effect of the blade tip clearance on the structure

Figure 9 shows the effect of the tip clearance on the stress and strain along the axial length of the rotor blade. The results indicate that the stress and strain first decrease and then increase with an increase in the axial length at a given tip clearance. However, the stress and strain decrease considerably with an increase in the tip clearance. The results show that the maximal values of the stress and strain are significantly affected by the tip clearance (Table 6). The trends are similar those shown in Figure 9.

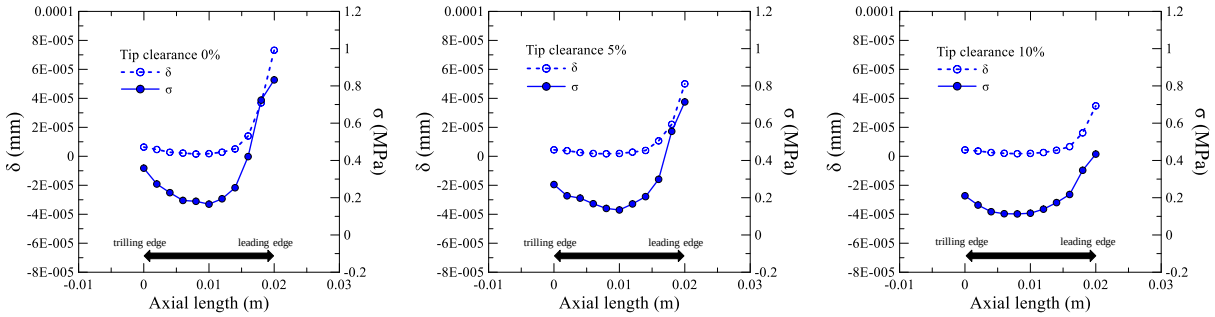

Figure 9 The structural analysis of the blade at difference tip clearances.

Table 6 Maximal and minimal value of stress and strain at different tip clearances.

	Stress (MPa)		Strain (mm)	
Items	Max.	Min.	Max.	Min.
Tip clearance 0%	8.323E-01	3.798E-01	7.318E-05	6.325E-06
Tip clearance 5%	7.140E-01	2.706E-01	5.000E-05	4.460E-06
Tip clearance 10%	4.339E-01	2.102E-01	3.482E-05	4.404E-06

The stress and strain of the leading edge are higher than those of the trilling edge at a given tip clearance. This is because the thickness of the rotor leading edge is smaller than that of the trilling edge. Figure 10 shows that the area of the affected stress can be reduced by increasing the tip clearance.

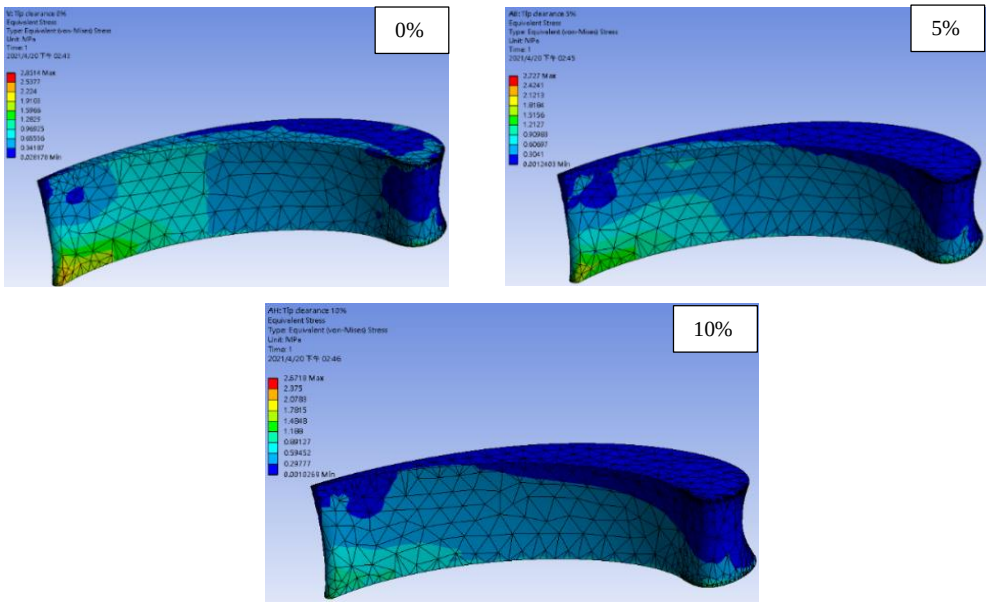

Figure 10 Stress contour on the rotor blade.

5 Conclusions

In this study, the effect of the tip clearance, which is the gap between the rotor tip and casing, on the performance and strength of the blade of the rotor, was investigated. The results showed that the turbine performance decreased and the strength of the blade increased with an increase in the tip clearance. Furthermore, the decay degree of the performance and strength improvement was low when the tip clearance was increased from 5% to 10%. The impact of the tip clearance on the isentropic efficiency and structure was higher in the range of 0-5% than that in range of 5-10%. Additionally, the strain and stress were related to the thickness of the blade of the rotor. The simulated results showed that, as the axial length increased, the stress and strain were high because the blade

was close to the leading edge.

6 Reference

1. Le V L, Kheiri A, Feidt M, Pelloux Prayer S. Thermodynamic and economic optimization of a waste heat to power plant driven by a subcritical ORC (Organic Rankine Cycle) using pure or zeotropic working fluid, Energy, 2014;78:622-38.
2. Chang J-C, Chang C-W, Hung T-C, Lin J-R, Huang K-C. Experimental study and CFD approach for scroll type expander used in low-temperature Organic Rankin Cycle. Appl Therm Eng 2014;73:1444-1452.
3. Papes I, Degroote J, Vierendeels J. New insights in twin screw expander performance for small scale ORC system from 3D CFD analysis. Appl Therm Eng 2015;91:535-46.
4. Sadiq G A, Tozer G, Dadah R-A, Mahmoud S. CFD simulation od compressed air two stage rotary Wankel expander-Parametric analysis. Energ Convers Manage. 2017;142:42-52.
5. Li. Y, Ren. X-D. Investigation of the organic Rankine cycle (ORC) system and the radial-inflow turbine design. Appl Therm Eng 2016;96:547-554.
6. AI Jubori AM, AI-Dadah RK, Mahmoud S, Daabo A. Modelling and parametric analysis of small-scale axial and radial outflow turbines for Organic Rankine Cycle applications. Appl Energ 2017;190:981-996.
7. Fiaschi D, Innocenti G, Manfrida G, Maraschiello F. Design of micro radial turbo expanders for ORC power cycles: From 0D to 3D. Appl Therm Eng 2016;99:402-410.
8. Wu. T, Shao. L, Yu. L, Wei. X, Ma. X, Zhang G. Design and structure optimization of small-scale radial inflow turbine for organic Rankine cycle system. Energy Convers and Manage 2019;199:111940.
9. Song. J, Gu. C-W, Ren. X. Influence of the radial-inflow turbine efficiency prediction on the design and analysis of the Organic Rankine Cycle (ORC) system. Energ Convers Manage 2016;123:308-316.
10. Lemmon, E.W., Huber, M.L., Mc. Linden, M.O, 2010, NIST Standard Reference Database 23: Reference Fluid Thermodynamic and Transport Properties REFPROP, Version 9.0, National Institute of Standards and Technology, Standard Reference Data Program, Gaithersburg, USA.

ACKNOWLEDGMENTS

The authors gratefully acknowledge the financial support provided for this study by the Ministry of Science and Technology of the Republic of China under MOST 108-2221-E-167-007-MY3.